Quasiparticle-Like Resonances and Spectral Inhomogeneity on the Surface of $Li_{0.9}Mo_6O_{17}$

Samuel Detmer,[1] Anjan Soumyanarayanan,[2,3] Michael M. Yee,[1] Yang He,[1] Martha Greenblatt,[4] Nigel E. Hussey,[5] and Jennifer E. Hoffman[1,6,*]

[1] *Department of Physics, Harvard University, Cambridge, Massachusetts 02138, USA*
[2] *Institute of Materials Research and Engineering, A*STAR, Singapore 138634*
[3] *Department of Physics, National University of Singapore, Singapore*
[4] *Department of Chemistry and Chemical Biology, Rutgers University, 123 Bevier Rd., Piscataway, NJ 08854, USA*
[5] *School of Physics, University of Bristol, Beacon House, Queens Road, Bristol, BS8 1QU, UK*
[6] *School of Engineering & Applied Sciences, Harvard University, Cambridge, Massachusetts 02138, USA*

(Dated: April 20, 2021)

The marked deviation from Fermi liquid behavior for the quasi-one-dimensional (1D) purple bronze $Li_{1-x}Mo_6O_{17}$ ($Li_{0.9}Mo_6O_{17}$) has generated much theoretical interest and has been observed by both bulk transport and surface-sensitive spectroscopic probes. Here we present spectroscopic scanning tunneling microscope (STM) images of 1D chains of molybdenum oxide units on the surface of $Li_{0.9}Mo_6O_{17}$. We find that the Coulomb suppression of tunneling around the Fermi energy is inhomogenous on the nanometer length scale, corresponding to inhomogeneity in the topography. Furthermore, we report that chains on the surface exhibit quasi-particle resonances at varying energies in their local density of states. These resonances break the particle-hole symmetry of the Tomonaga-Luttinger liquid model. We discuss the implications of this phenomenon for modeling the surface structure of $Li_{0.9}Mo_6O_{17}$ as a quasi-1D quantum system.

I. INTRODUCTION

1 **[Luttinger liquids are interesting]** Although Fermi-liquid theory satisfactorily describes electron behavior in typical conducting solids, quasi-one-dimensional (1D) materials exhibit unique properties that are currently best understood within the framework of Luttinger liquid theory. Luttinger liquid theory provides the best low-energy effective description for a diverse array of physical models [1] and has notably contributed to the study of the fractional quantum Hall effect [2] and to the description of the normal states of high-temperature superconductors [3]. As rare alternatives to the predictions of Fermi-liquid theory, the unique properties of Luttinger liquids continue to warrant extensive theoretical and experimental study in the recent literature. [4–12]. In particular, scanning tunnelling microscopy (STM) has proven to be a powerful technique for studying Luttinger liquids' departure from the Fermi-liquid model. Recent STM experiments have confirmed several unique 1D behaviors in Luttinger liquids, including a lack of quasiparticle resonances and a power-law suppression of density of states near the Fermi energy.

2 **[1D to 3D transition in LMO poorly understood]** $Li_{0.9}Mo_6O_{17}$ is one among a family of purple bronze materials whose crystal structure comprises zigzag chains of MoO_6 octahedra[13]. These octahedral chains are expected to dominate the electronic behavior of $Li_{0.9}Mo_6O_{17}$, which is found to be strongly anisotropic with respect to its crystallographic axes. Transport studies have established that its quasi-1D transport characteristics are consistent with Tomonaga Luttinger liquid (TLL) behavior, including unconventional quasiparticles, and the separation of their spin and charge degrees of freedom. As its temperature is reduced, $Li_{0.9}Mo_6O_{17}$ is found to undergo a metal-to-insulator transition at $\sim$ 25 K, variously attributed to dimensional crossover, CDW, and localization. This is followed by the onset of superconductivity at $\sim$ 2 K, which is expected to have an unconventional spin triplet mechanism[14, 15]. Previous spectroscopic work has characterized the purple bronze $Li_{0.9}Mo_6O_{17}$ as a model 1D system for studying Luttinger theory, suggesting a Coulomb suppression of density of states around the Fermi energy [16]. However, the effect of electronic inhomogeneity on the spectroscopic properties remains to be investigated.

3 [] Here we report STM evidence that the disordered surface of $Li_{0.9}Mo_6O_{17}$ at low temperature is not fully described by the bulk Luttinger-liquid model, despite having spatially-averaged properties that are consistent with the 1D theory. In fact, our study of a disordered *b*-*c* crystal surface of $Li_{0.9}Mo_6O_{17}$ shows three ways in which its energetic spectrum is spatially disordered: the width of the Coulomb gap, the value of the Luttinger-liquid alpha parameter, and the energies and intensities at which resonance peaks appear in the local density of states. We observed these resonance peaks frequently in the local density of states (LDOS) spectra at various points on the $Li_{0.9}Mo_6O_{17}$ surface. The resonances appear to exhibit lifetime broadening, consistent with a Fermi-liquid theory. We also observed that the value of α and the consistency of the Coulomb gap varied dramatically from point to point on the surface, even in the absence of resonances. Inhomogeneities on the surface of $Li_{0.9}Mo_6O_{17}$ have been

* jhoffman@physics.harvard.edu

mentioned elsewhere [16], but previous literature has not yet produced a detailed experimental study, nor have any quasiparticle-like resonances on the surface been previously noted. In fact, earlier STM studies have focused on spectra averaged over a $Li_{0.9}Mo_6O_{17}$ surface [11, 16]. The inhomogeneities in LDOS spectra on $Li_{0.9}Mo_6O_{17}$ that we observe are significant for understanding the 1D to 3D transition of $Li_{0.9}Mo_6O_{17}$ at low temperature as well as the response of Luttinger-liquids to impurities and boundary conditions.

II. SURFACE CHARACTERIZATION

4 **[Materials and Methods]** Data was collected using a home-built STM at a temperatures of 4 K or 6 K. We cleaved single crystals of $Li_{0.9}Mo_6O_{17}$ in cryogenic ultra-high vacuum *in situ* and inserted them directly into the STM. Measurements were performed with a mechanically cut Pt-Ir tip, which was cleaned by field emission and characterized on gold. Spectroscopy was conducted using a lock-in technique at 1.115 kHz. Topographic and spectroscopic properties of the 1D chains were verified using several tips.

5 **[Surface Identification]** We characterized our surface as the *b*-*c* crystal plane of $Li_{0.9}Mo_6O_{17}$ using topographic maps. The lattice parameters were measured by Fourier analysis of 30 topographic scans, as shown in Figure 1. We found Bragg peaks for $b = 0.58 \pm 0.06$ nm and $c = 0.98 \pm 0.17$ nm, agreeing with the neutron scattering measurements for the lattice parameters of $Li_{0.9}Mo_6O_{17}$ within our uncertainty [13]. We observe that our surface showed various reconstructions and that chains are clearly visible despite the presence of nanometer scale disorder. There are four possible crystal planes which we could have exposed: Mo1, Mo2-Mo4, Mo3-Mo5, and Mo6 [11]. Based on the presence of alternating light and dark chains in the topographic scans which indicate the presence of two inequivalent types of Mo atoms, we expect to have revealed either the Mo2-Mo4 or Mo3-Mo5 planes.

The general spectral features that we observe on a 10 nm scale are consistent with the results of former experimental literature. We obtained spectra from points on the surface using the proportionality of the differential conductance of tunneling to the local density of states.

6 **[Average spectroscopic features, α fit]** The spatially-averaged spectrum of our samples agrees with a previous report [18] and is shown in Figure 2. Consistent with earlier results, our average spectra show band features around ± 200 mV, as predicted by DFT calculations [4]. Our spatially-averaged spectrum also appears to show a Coulomb suppression of tunneling around the Fermi energy, which we henceforth refer to as a Coulomb gap. We used double-log scale plots of the data to extract the value of the Luttinger liquid parameter α from the spatially-averaged spectrum. We found $\alpha \approx 0.44$, in agreement with earlier results for averaged spectra on

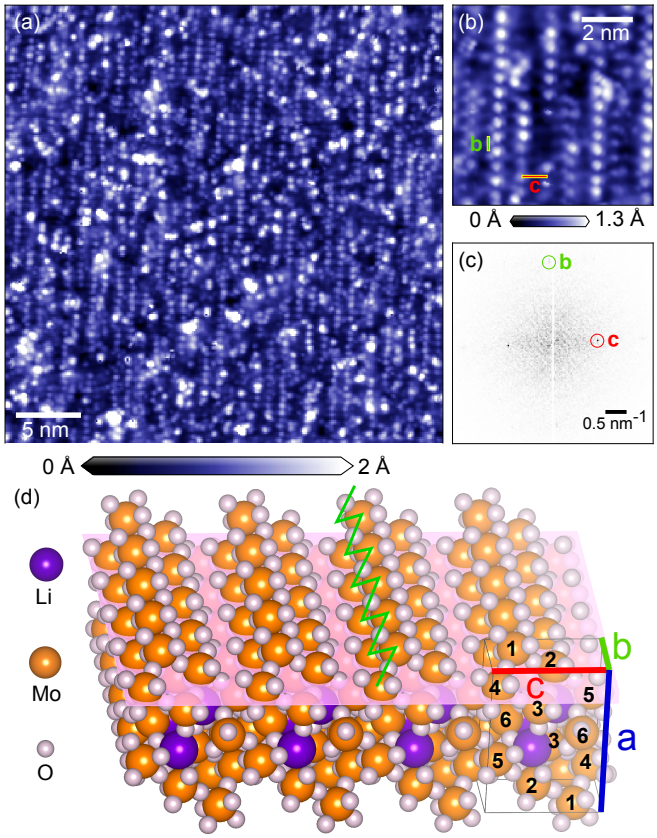

FIG. 1. Surface identification. (a) Topographic map showing chains of molybdenum oxide clusters in LPB at $T = 4.8$ K. A linear fit to the background was subtracted in both topographs in this figure. (b) 7 nm topograph of a different surface showing the interatomic spacing in more detail. (c) Fourier transform of the 30 nm topograph in Figure 1a, with circled peaks corresponding to the lattice vectors. (d) Crystal structure of the b-c plane of LPB showing a lattice plane parallel to that in topographs (a) and (b). Crystal structure coordinates are from [13] and image was produced with VESTA [17]. Setpoint parameters: sample bias, $V_s = -400$ mV (a and b); junction resistance, $R_J = 40$ GΩ (a) and -20 GΩ (b).

$Li_{0.9}Mo_6O_{17}$ within uncertainty [16, 18].

7 **[Variation of Coulomb gap]** Despite the agreement of the spatially-averaged spectrum with previously reported results for $Li_{0.9}Mo_6O_{17}$, the spatially resolved results show significant spectral inhomogeneity. Specifically, the shape and width of the Coulomb gap varies substantially across the surface. We identified edges of the Coulomb gap as minima in the second derivative corresponding to kinks in the local density of states spectrum below and above the Fermi energy for individual points in our data set. The distance from the Fermi energy to the gap edge on the hole side was not strongly correlated with the distance from the Fermi energy to the gap edge on the particle side. Spectra with the same values of positive or negative gap edge tended to occur in chains that

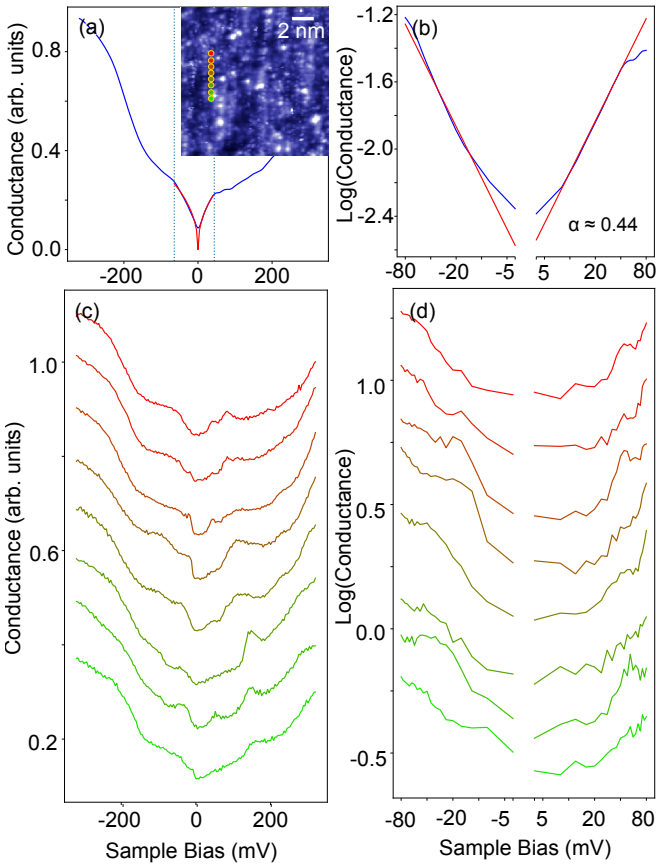

FIG. 2. Spatial inhomogeneity of spectra. (a) Average spectrum over the region shown in inset. *Inset*: 30 nm topograph of the a-b crystal plane of $Li_{0.9}Mo_6O_{17}$. The Coulomb gap is delimited by dashed lines. A power law fit ($\alpha = 0.44$) is shown in red. (b) Log-log plot of average spectrum in 2a. (c) Waterfall plot showing variance in the size and shape of the Coulomb gap along the yellow line shown in the inset to 2a. (d) Log-log plot of graph in 2c showing variance in the size and shape of the Coulomb gap along the red line shown in Figure 2a. Setpoint Parameters for spectra in 2b, 2c, and 2d (S) and for topograph in 2a (T): sample bias, $V_s = -400$ mV (S) and 100 mV (T); junction resistance, $R_J = 1.6$ GΩ (S) and 10 GΩ (T); and root mean square (RMS) lock-in excitation, $V_{rms} = 6$ mV (S). Temperature: $T = 6$ K (S) and 4.8 K (T).

resembled the chains of atoms in the topography.

8 [**Variation of** α] The Luttinger-liquid alpha parameter also varies across the $Li_{0.9}Mo_6O_{17}$ surface. Log-log plots of point spectra, which are expected to be linear near the Fermi energy for a Luttinger liquid, display highly nonlinear behavior (Figure 2d). Attempting to fit these lines with a power-law exponent results in a variety of different α values at different points on the surface.

III. RESONANCES

9 [**General resonance phenomenology**] The surface of $Li_{0.9}Mo_6O_{17}$ exhibits frequent resonance peaks in the LDOS. These resonances manifest in conductance maps as shown in Figure 3c-h and correlate to chain-like features in the topography. These resonance peaks have not been observed before in $Li_{0.9}Mo_6O_{17}$ but are quite common on the surfaces that we studied. In the topography shown in Fig. 3, more than 50% of the roughly 83,000 point spectra exhibited clearly identifiable resonances in their LDOS. Resonances can occur on both the particle and hole sides of the spectrum, but appear on the particle side with greater frequency. Many resonant spectra contain more than one resonance peak, some containing up to three distinct resonance peaks on the same side of the Fermi energy. Spectra exhibiting resonances are generally particle-hole asymmetric. Most of the resonances appear in the energy range −100 mV to 100 mV.

10 [**Resonances occur in chains**] Most of the resonances appear in chain-like patterns that correspond to the topographic features on the $Li_{0.9}Mo_6O_{17}$ surface. The conductance maps in Figure 3 demonstrate this chain-like behavior in the local density of states at fixed energies across the surface. The features in these conductance maps presumably show chains of atoms resonating at different energies. In addition to these chain resonances, we sometimes observe additional peaks corresponding to unique resonances at each location along the chain. Thus, a given unit cell of $Li_{0.9}Mo_6O_{17}$ that is observed in the topography may contain both a large resonance peak that is common to all of its neighbors and some smaller resonances that are unique to itself.

11 [**Code to identify chains**] The fact that resonances appear close together in linear patterns allows them to be grouped together as chains. We used a custom code to select points that resonated at the same energy and then group them into features. Over 400 groups of resonances were identified in this way. The output is shown overlaid on the topography in Figure 4a. Although the chains tend to form clusters that resonate at similar energies, there are also a number of cases where two chains resonating at different energies are close to one another. We restricted our search for chains to those with resonances between −120 mV and 120 mV, because most of the resonances identified occurred within those boundaries.

12 [**Chain length**] Identifying chains also allowed us to obtain an approximate value for the spatial lengths of the resonance features. Figure 4c shows the frequency at which chains of a certain length resonate at a particular energy. Although there may be a slight average trend toward longer chains resonating at lower energies, noise in the data renders it impossible to draw a statistically significant conclusion. Details about the algorithms used to find chains and compute their length are contained in the Supplemental Material.

13 [**Lifetime broadening**] The resonances that we

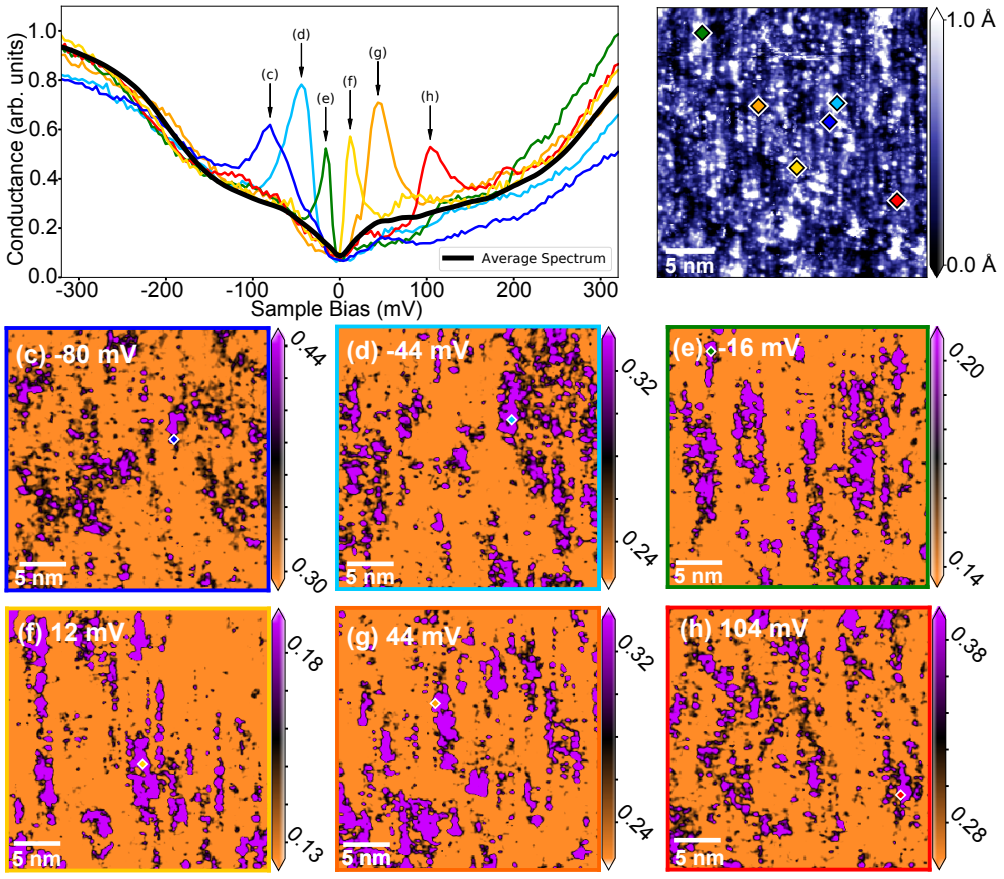

FIG. 3. Characterization of resonances. (a) Sample of resonances peaks at various energies, corresponding to points labelled by the colored diamonds in Figure 3b. The spectral average over the entire surface is also displayed (bolded black line). (b) Topograph showing points where the resonances from Figure 3a are observed. (c)-(h): Conductance maps showing chain-like resonances at various energies. These conductance maps are shown after spatial smoothing using a Gaussian with $\sigma = 0.104$ nm corresponding to one pixel of spatial resolution. Setpoint parameters for spectra in 3a and 3c-3h (S) and for topograph in 3b (T): $V_s = -400$ mV (S) and 100 mV (T); $R_J = 1.6$ GΩ (S) and 10 GΩ (T); $V_{\text{rms}} = 6$ mV (S). Temperature: $T = 6$ K (S) and 4.8 K (T).

observe tend to become broader at energies farther away from the Fermi energy, in both the particle and the hole directions. The spectral resonances fit well to a Lorentzian lineshape, given by

$$L(x) = \frac{A}{\pi} \frac{\frac{1}{2}\Gamma}{(x - x_0)^2 + \left(\frac{1}{2}\Gamma\right)^2}, \qquad (1)$$

where A is the resonance amplitude and Γ the full-width at half-maximum (FWHM). Using this formula, we calculated full-widths at half-maxima for resonance features at each energy, averaged over points within a chain grouping. Figure 4b shows the result. We observe a clear increase in the width of resonances as the resonance energy moves away from the Fermi energy, also known as lifetime broadening. Lifetime broadening is typically associated with three-dimensional phenomena and is particularly reminiscent of Fermi-liquid quasiparticle signatures in LDOS spectra.

IV. DISCUSSION

14 **[Inhomogeneity relevance for bulk]** The new properties that we report for the $Li_{0.9}Mo_6O_{17}$ surface, in particular the presence of quasiparticle-like resonances at low energy, show that the traditional Luttinger liquid model is not adequate for fully explaining the electronic properties of a disordered low-temperature $Li_{0.9}Mo_6O_{17}$ surface. A feature resembling a charge gap was still observed at most sites, showing that some features resembling Luttinger behavior were present in our study. Nevertheless, Luttinger parameters such as the gap width and α parameter did very across the surface, most likely due to the presence of impurities and surface disorder. As has been noted by DFT calculations, the properties of $Li_{0.9}Mo_6O_{17}$ are very sensitive to lithium stoichiometry [8]. The sensitivity of $Li_{0.9}Mo_6O_{17}$ to exact stoichiometry may cause the spectral behavior of $Li_{0.9}Mo_6O_{17}$ chains to change in the presence of surface reconstructions such as those observed on our $Li_{0.9}Mo_6O_{17}$ surface. Variation

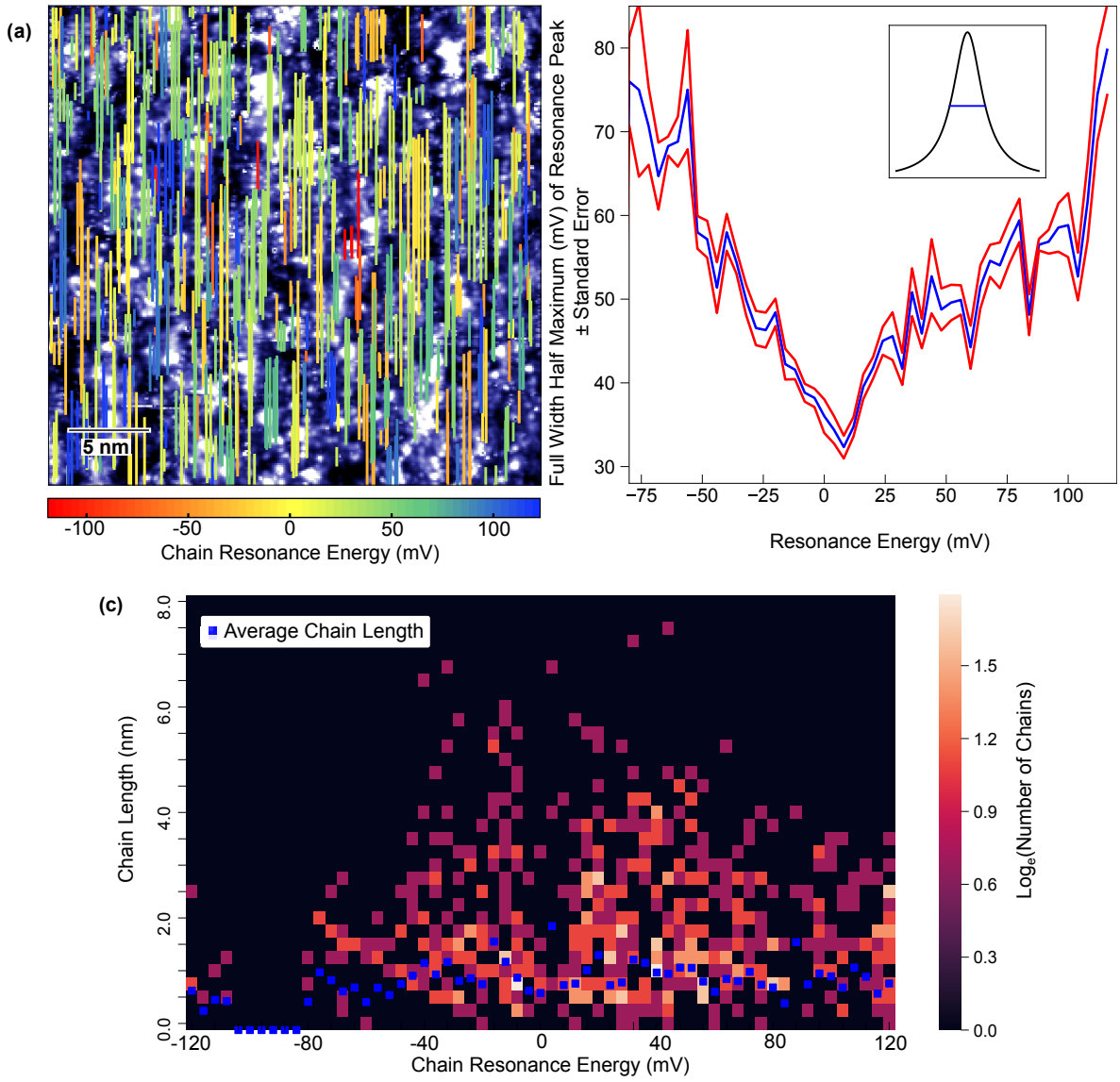

FIG. 4. Chain analysis. (a) Chains identified by software (see Supplemental Information) are shown superposed on the surface topograph. The color of the chains corresponds to the sample bias at the chain resonance peak. (b) The average FWHM (full width at half maximum) of Lorentzian fits to chain resonance peaks is shown in blue, as a function of chain resonance energy. The red lines denote one standard error above and below the mean. (c) A logarithmic heat map shows the number of chains of given length and resonance energy. The average chain length at each resonance energy is shown by the scatter plot of blue squares.

in the bulk concentration of Li atoms may lead to effects similar to those observed on the material's surface, but spatial inhomogeneity in the spectral properties of $Li_{0.9}Mo_6O_{17}$ on its surface may also be consistent with the Luttinger model in the bulk.

15 **[Fermions vs. bosons, particle-hole symmetry]** On the other hand, quasiparticle-like resonances in $Li_{0.9}Mo_6O_{17}$ do not fit the conventional Luttinger liquid model. Traditional quasiparticle resonances indicate the presence of fermionic bound states, whereas Luttinger liquids are expected to exhibit bosonic collective excitations. Additionally, the quasiparticle resonances that we observed break the particle-hole symmetry of the Luttinger liquid model around the Fermi energy. This suggests the need for a revision to the Luttinger liquid model to describe $Li_{0.9}Mo_6O_{17}$ chains on a disordered surface. Quasiparticle resonances may arise from scattering of fermionic bound states off of impurities, as has been proposed for similar chain-like resonances observed in $YBa_2Cu_3O_{6+x}$ [19]. An alternate explanation for these resonances in terms of a modified Luttinger theory would need to account for resonances on both the particle and hole sides of the spectrum, as well as for the comparatively large width of resonance peaks that we observe. By

providing a picture of the formation of quasiparticle-like resonances in 1D systems, this research may help to elucidate the elusive mechanism behind the 1D to 3D transition of $Li_{0.9}Mo_6O_{17}$ at low energies and provide further insight into the properties of this unique material.

[1] F. D. M. Haldane, 'Luttinger liquid theory' of one-dimensional quantum fluids. I. properties of the Luttinger model and their extension to the general 1D interacting spinless Fermi gas, Journal of Physics C: Solid State Physics **14**, 2585 (1981).

[2] X. G. Wen, Chiral Luttinger liquid and the edge excitations in the fractional quantum Hall states, Physical Review B **41**, 12838 (1990).

[3] P. W. Anderson, 'Luttinger-liquid' behavior of the normal metallic state of the 2D Hubbard model, Physical Review Letters **64**, 1839 (1990).

[4] Z. S. Popović and S. Satpathy, Density-functional study of the Luttinger liquid behavior of the lithium molybdenum purple bronze $Li_{0.9}Mo_6O_{17}$, Physical Review B **74**, 045117 (6) (2006).

[5] H. Chen, J. J. Ying, Y. L. Xie, G. Wu, T. Wu, and X. H. Chen, Magnetotransport properties in purple bronze $Li_{0.9}Mo_6O_{17}$ single crystal, EPL (Europhysics Letters) **89**, 67010 (2010).

[6] N. Wakeham, A. F. Bangura, X. Xu, J.-F. Mercure, M. Greenblatt, and N. E. Hussey, Gross violation of the Wiedemann-Franz law in a quasi-one-dimensional conductor, Nature Communications **2**, 396 (2011).

[7] M. S. da Luz, J. J. Neumeier, C. A. M. dos Santos, B. D. White, H. J. I. Filho, J. B. Leão, and Q. Huang, Neutron diffraction study of quasi-one-dimensional lithium purple bronze: Possible mechanism for dimensional crossover, Physical Review B **84**, 014108 (2011).

[8] P. Chudzinski, T. Jarlborg, and T. Giamarchi, Luttinger-liquid theory of purple bronze $Li_{0.9}Mo_6O_{17}$ in the charge regime, Physical Review B **86**, 075147 (2012).

[9] L. Dudy, J. D. Denlinger, J. W. Allen, F. Wang, J. He, D. Hitchcock, A. Sekiyama, and S. Suga, Photoemission spectroscopy and the unusually robust one-dimensional physics of lithium purple bronze, Journal of Physics: Condensed Matter **25**, 014007 (2013).

[10] M. Nuss and M. Aichhorn, Effective model for the electronic properties of quasi-one-dimensional purple bronze $Li_{0.9}Mo_6O_{17}$ based on ab initio calculations, Physical Review B **89**, 045125 (2014).

[11] L. Fu, A. M. Kraft, M. Greenblatt, and M. C. Boyer, Origin of a superlattice observed in $Li_{0.9}Mo_6O_{17}$ by scanning tunneling microscopy, Physical Review B **93**, 045430 (2016).

[12] P. Chudziński, Multi-orbital physics in lithium-molybdenum purple-bronze: going beyond paradigm, The European Physical Journal B **90**, 148 (2017).

[13] M. Onoda, K. Toriumi, Y. Matsuda, and M. Sato, Crystal structure of lithium molybdenum purple bronze $Li_{0.9}Mo_6O_{17}$, Journal of Solid State Chemistry **66**, 163 (1987).

[14] J.-F. Mercure, A. F. Bangura, X. Xu, N. Wakeham, A. Carrington, P. Walmsley, M. Greenblatt, and N. E. Hussey, Upper critical magnetic field far above the paramagnetic pair-breaking limit of superconducting one-dimensional $Li_{0.9}Mo_6O_{17}$, Physical Review Letters **108**, 187003 (2012).

[15] A. G. Lebed and O. Sepper, Possible triplet superconductivity in the quasi-one-dimensional conductor $Li_{0.9}Mo_6O_{17}$, Physical Review B **87**, 100511 (2013).

[16] J. Hager, R. Matzdorf, J. He, R. Jin, D. Mandrus, M. A. Cazalilla, and E. W. Plummer, Non-Fermi-liquid behavior in quasi-one-dimensional $Li_{0.9}Mo_6O_{17}$, Physical Review Letters **95**, 186402 (2005).

[17] K. Momma and F. Izumi, VESTA 3 for three-dimensional visualization of crystal, volumetric and morphology data, Journal of Applied Crystallography **44**, 1272 (2011).

[18] T. Podlich, M. Klinke, B. Nansseu, M. Waelsch, R. Bienert, J. He, R. Jin, D. Mandrus, and R. Matzdorf, Luttinger liquid behaviour of $Li_{0.9}Mo_6O_{17}$ studied by scanning tunnelling microscopy, Journal of Physics: Condensed Matter **25**, 014008 (2013).

[19] D. J. Derro, E. W. Hudson, K. M. Lang, S. H. Pan, J. C. Davis, J. T. Markert, and A. L. de Lozanne, Nanoscale one-dimensional scattering resonances in the CuO chains of $YBa_2Cu_3O_{6+x}$, Physical Review Letters **88**, 097002 (2002).

Supplemental Information for

Quasiparticle-Like Resonances and Spectral Inhomogeneity on the Surface of $Li_{0.9}Mo_6O_{17}$

Samuel Detmer, Anjan Soumyanarayanan, Michael M. Yee, Yang He, Martha Greenblatt, Nigel E. Hussey, and Jennifer E. Hoffman*

I. RESONANCE FINDER ALGORITHM

To computationally identify resonances in individual point STM spectra, we used two criteria: a sharpness criterion, which distinguishes resonances from broader features in the spectra, and a height criterion, which ensures that random fluctuations in point spectra are not identified as resonances.

For a given point spectrum $A(E, r)$, we performed the following operations:

1. **Figure Ia:** Let $B(E)$ denote the spatial average of all the spectra we observed on the surface. Define a difference function $D(E, r) = A(E, r) - B(E)$. This shows how much our spectrum at A differs from a typical spectrum at each sample bias.

2. **Sharpness Criterion (Figure Ib):** For each sample bias E within the range -200 mV to 200 mV, define $M(E, r)$ to be the mean value of the difference function $D(E, r)$ in an energetic neighborhood of width 80 mV centered on E. [1]

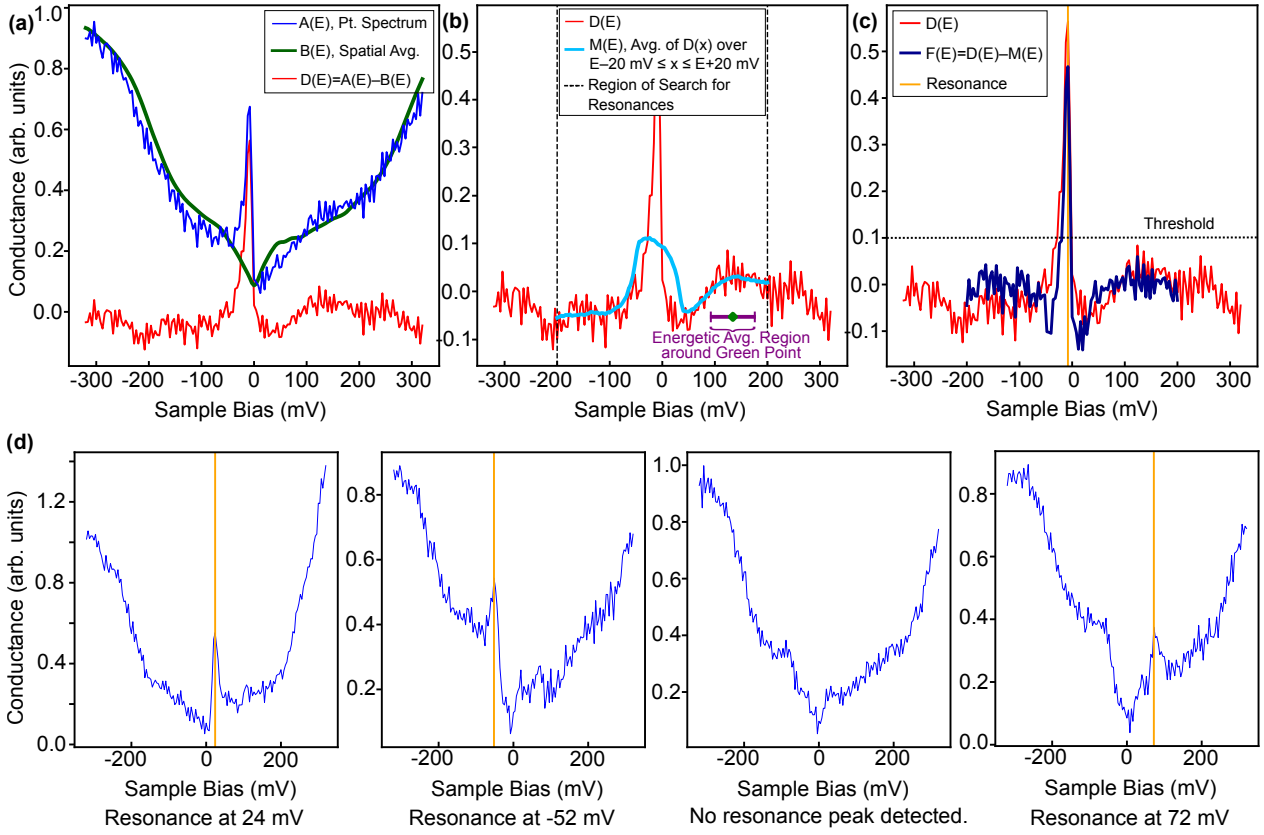

* jhoffman@physics.harvard.edu

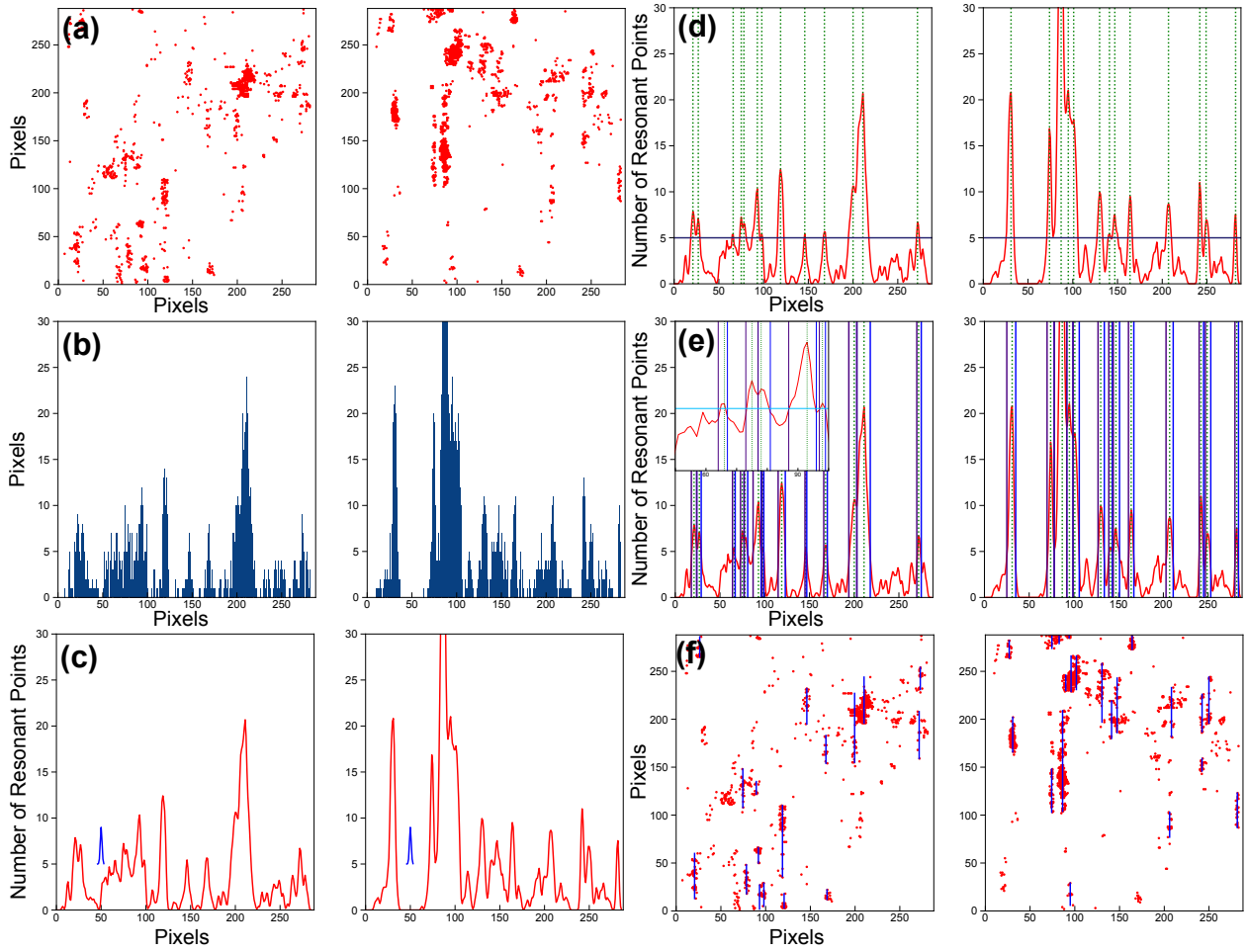

3. **Height Criterion (Figure Ic:):** Define $F(E,r) = D(E,r) - M(E,r)$ for $|E| \leq 200$ mV. $F(E,r)$ represents how much the difference function $D(E,r)$ at E is above or below the average value of D for energies around E. Maxima of $F(E,r)$ thus correspond to values of the spectrum $A(E,r)$ that exceed the spatially-averaged spectrum by more than the points around them do. We limit our finder to one resonance peak per spectrum $A(E,r)$ by finding the E for which $F(E,r)$ is a global maximum. If $F(E,r) \geq 0.1$, return E as the resonance energy for this point. If $F(E,r) < 0.1$, report that no resonance was found.

   Figure Id provides examples of the resonanceFinder's operation.

II. CHAIN FINDER ALGORITHM

In the following description, we label the pixels of our image with a discrete set of x-coordinates and y-coordinates. To find the chains that resonate at sample bias E:

1. **Figure IIa:** First, identify all of the points P that have resonances at E.
2. **Figure IIb:** Make a histogram $Z(x,E)$ of the x-values of these points P.
3. **Figure IIc:** Smooth the histograms with a Gaussian of width (standard deviation) 1 pixel.
4. **Figure IId:** Find local maxima of the smoothed histograms. Specifically, look for x-values that meet the following criteria:
   (a) $Z(x,E) > 5$. (The value of Z, or histogram, represents how many resonant points have a given x-coordinate.)
   (b) $Z(x,E) > Z(x-1,E)$ and $Z(x,E) > Z(x+1,E)$.

(c) $x \neq \min(x)$ and $x \neq \max(x)$ [so that condition (b) can be tested].

5. **Figure IIe:** Find regions around the local maxima that correspond to the widths of chain features. Let us denote the x-values of the local maxima that we found in step 5 as $X_1, X_2, \ldots, X_N$. We find the lower boundary and upper boundary (in x-coordinates) of the chain-width region around a given local maximum X_i in the following way: To find the upper boundary, we start with k=1 and check whether the x-value $X_i + k$ meets all of the following criteria:

   (a) $Z(X_i + k, E) > 5$. (There are more than five resonant points that have x-value $X_i + k$.)
   (b) $Z(X_i + k, E) > Z(X_i + k + 1, E)$. ($X_i + k$ is not a local minimum or saddle point.)
   (c) $Z(X_i + k, E) \neq \max(x, E)$. ($X_i + k$ is not an endpoint of the x-axis).

   If $X_i + 1$ satisfies all these criteria, then we increment k by one and then check the criteria for $X_i + k$, where $k = 2$ in this case. We repeat this process until we find a value of $k = k_U + 1$ for which at least one of the criteria is not satisfied. Then we assign k_U to be the upper bound of the chain-like region around x_i. To find the lower boundary, we check whether the x-value X_i–k meets all of the following criteria:

   (a) $Z(X_i - k, E) > 5$. (There are more than five resonant points that have x-value X_k–1.)
   (b) $Z(X_i - k, E) < Z(X_i - k + 1, E)$. ($X_i - k$ is not a local minimum or saddle point).
   (c) $Z(X_i - k, E) \neq \min(x)$. ($X_i - k$ is not an endpoint of the x-axis).

   If X_i–1 satisfies all these criteria, then we increment k by one and then check the criteria for $X_i - k$, where $k = 2$ in this case. We repeat this process until we find a value of $k = k_L - 1$ for which at least one of the criteria is not satisfied. Then we assign k_L to be the lower bound of the chainlike region around x_i.

6. **Figure IIf:** We look at all of the points that resonate at E and that have x-values falling within the range $[X_i$–$k_L, X_i + k_U]$ for some local maximum X_i. Of all these points, we pick the point that has the lowest y-value and use this to start a protochain. We proceed to add points to this chain as long as they are no more than 15 pixels in y-coordinate above the previously added point. Once there are no points no more than 15 pixels above, we close the protochain. If the protochain contains fewer than 10 points, we discard it since there are not enough resonances to determine whether this is a physical feature. If the protochain contains more than 10 points, then we promote it to a chain and add it to our list. We then repeat the process, starting with the point that was more than 15 pixels above the last chain, until all the points at this x value have been considered as part of a protochain and either discarded or added to a chain.

—

We also tried an alternative method of finding chains, which produced worse results as verified below in Section III [2]

III. VERIFICATION AND STABILITY OF RESULTS

We verified our results over changes in the sharpness and height parameters for the Resonance Finder program and the minimum histogram height and vertical chain parameters for the Chain Finder program. The results are shown in Figures 1-5 below. The results show remarkable stability over the range of reasonable parameter space.

---

[1] We use the range −200 mV to 200 mV so that the resonanceFinder does not identify regions with pronounced increase in slope in the 200 to 320 mV range as resonance peaks, since they correspond rather to the general band structure of the material.

[2] ChainFinder: Description of Previous Method
First, we smoothed the data using a Gaussian with standard deviation =0.05 nm (resolution= 1 nm) on the spatial axes and $\sigma = 4$ mV (resolution= 4 mV) on the energy axis. We calculated local means and standard deviations for every 32 mV by 5 nm by 5 nm box in 3D space.
Then, we identified resonances by requiring a resonant peak to be simultaneously 1.5 spatial standard deviations above the spatial mean and 0.75 energy standard deviations above the energetic mean for the box centered on that peak. The parameters were determined in order to produce about 100,000 peaks. Varying the number of peaks and the parameters did not affect the shape of the average chain length versus energy plot, unless we obtained an insufficient number of peaks so that our sample size was too small. Code was implemented using matrix operators.

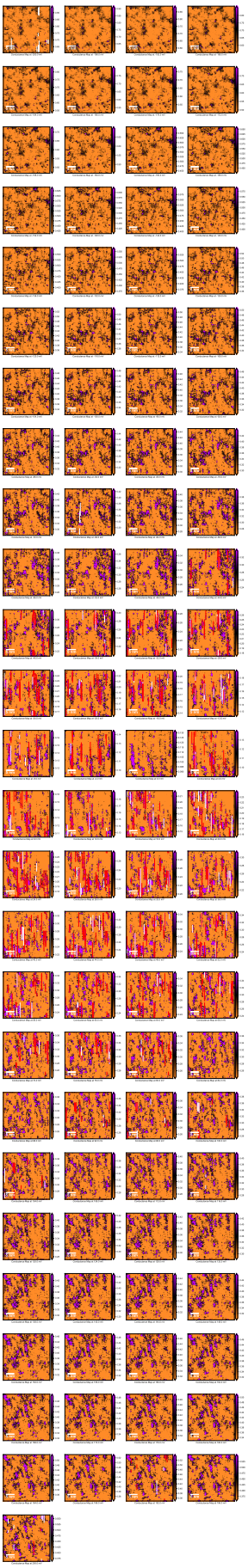

FIG. 1. Chain Finder Verification: Chains identified (red lines) shown overlaid on conductance maps at all bias voltages.

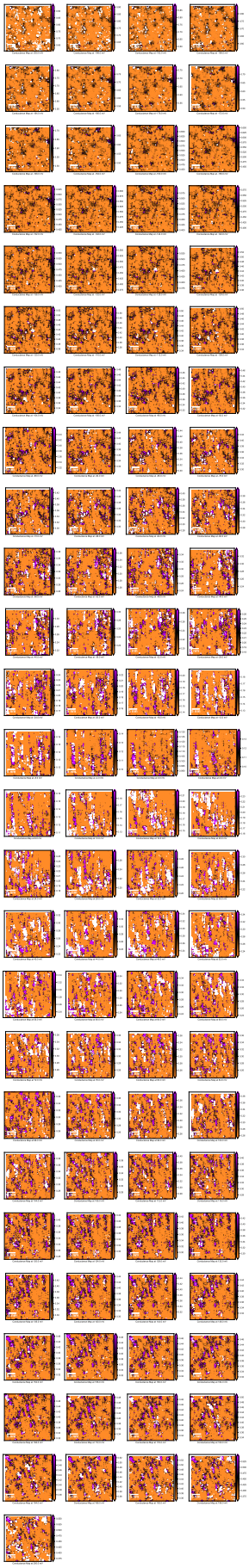

FIG. 2. Resonance Finder Verification: Resonances identified (white dots) shown overlaid on conductance maps at all bias voltages.

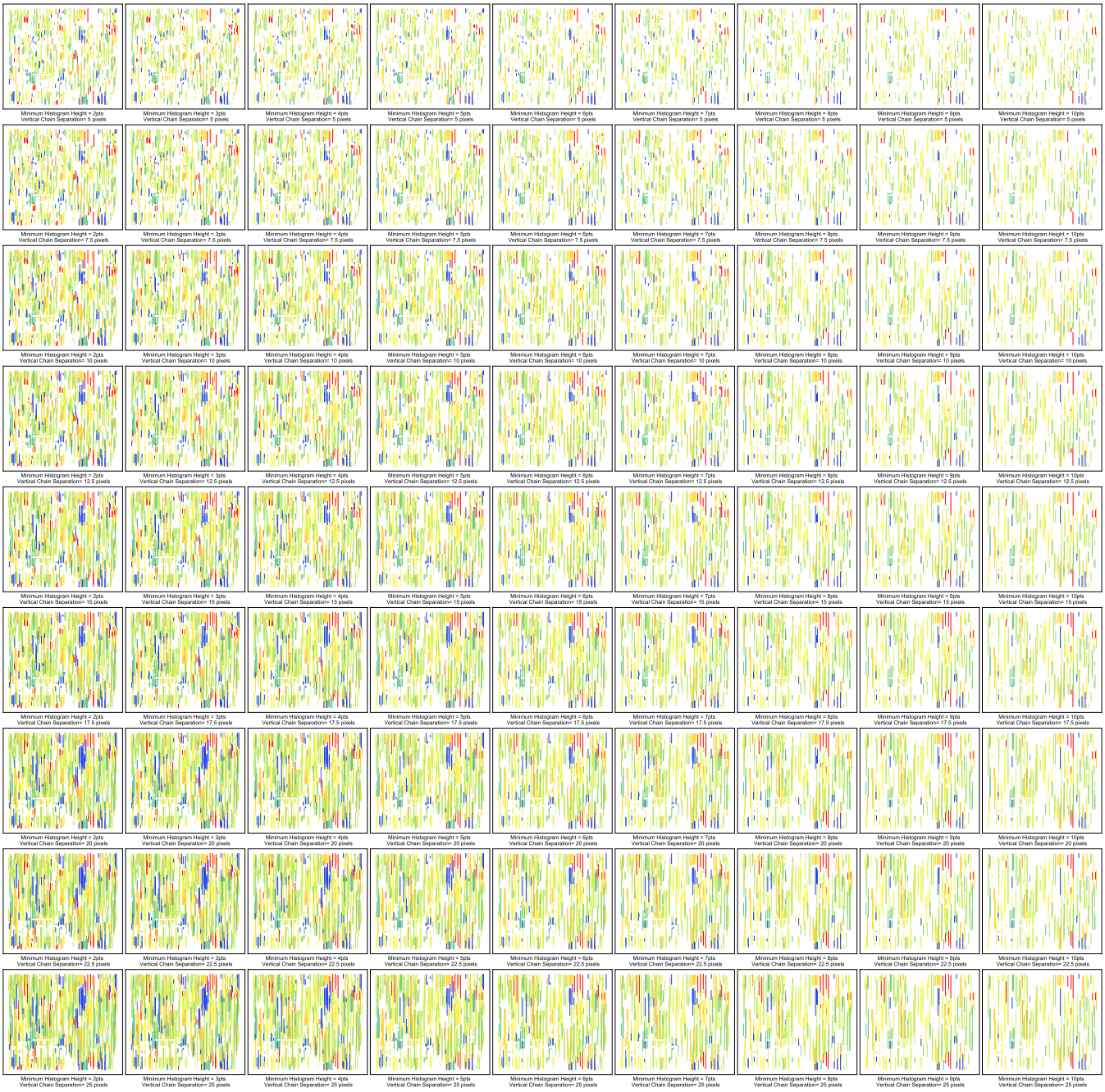

FIG. 3. Reproductions of Figure 4a using values of minimum histogram height (MHH) varying from 2 points (*left*) to 10 points (*right*) with vertical chain separation (VCS) varying from 5 pixels (*top*) to 25 pixels (*bottom*) in increments of 2.5 pixels. As the parameters become more and more restrictive (toward the upper right corner) fewer and fewer chains are identified, but the energies and locations of chains are remarkably consistent. The chain features, including number of chains, also appear to be especially consistent within the range of values that are reasonable (middle left-hand), whence the figures in the main text are derived.

Third, we grouped the resonance peaks into chains by identifying clusters of points with the following properties:
1) Each point in the group is no more than 1.5 nm away in the vertical direction and 0.3 nm away in the horizontal direction from at least one other point in the group.
2) The group contains at least 6 points.
3) If the group has a bimodal distribution (corresponding to two separate chains close to one another), the group is split along its two modes.

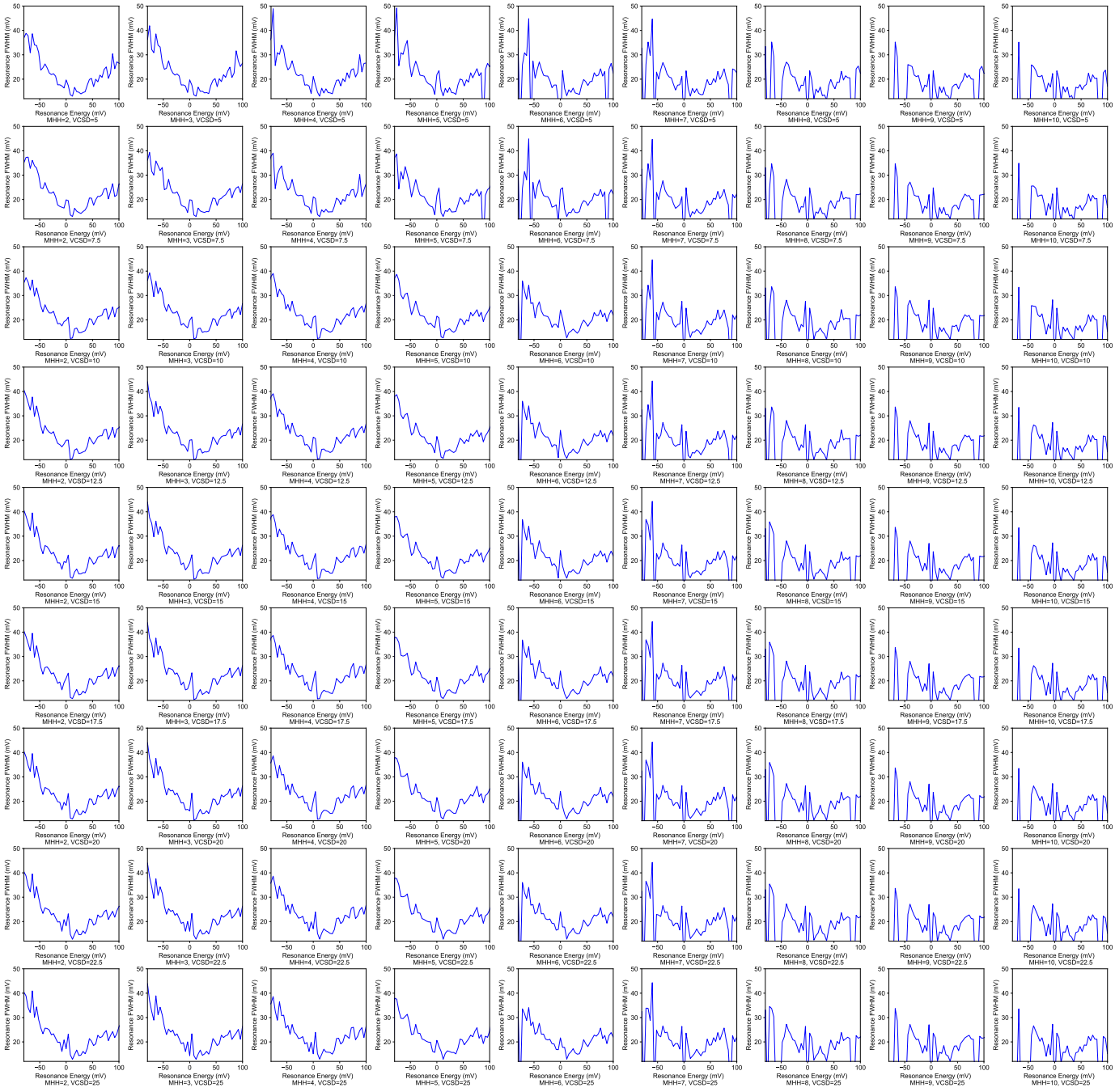

FIG. 4. Reproductions of Figure 4b using values of minimum histogram height (MHH) varying from 2 points (*left*) to 10 points (*right*) with vertical chain separation (VCS) varying from 5 pixels (*top*) to 25 pixels (*bottom*) in increments of 2.5 pixels. As the parameters become more and more restrictive (toward the upper right corner) fewer and fewer chains are identified, which leads to greater variation in the graphs shown. As in 4a, the main features appear to be especially consistent within the range of values that are reasonable (middle left-hand), whence the figures in the main text are derived. All figures show some degree of lifetime broadening.

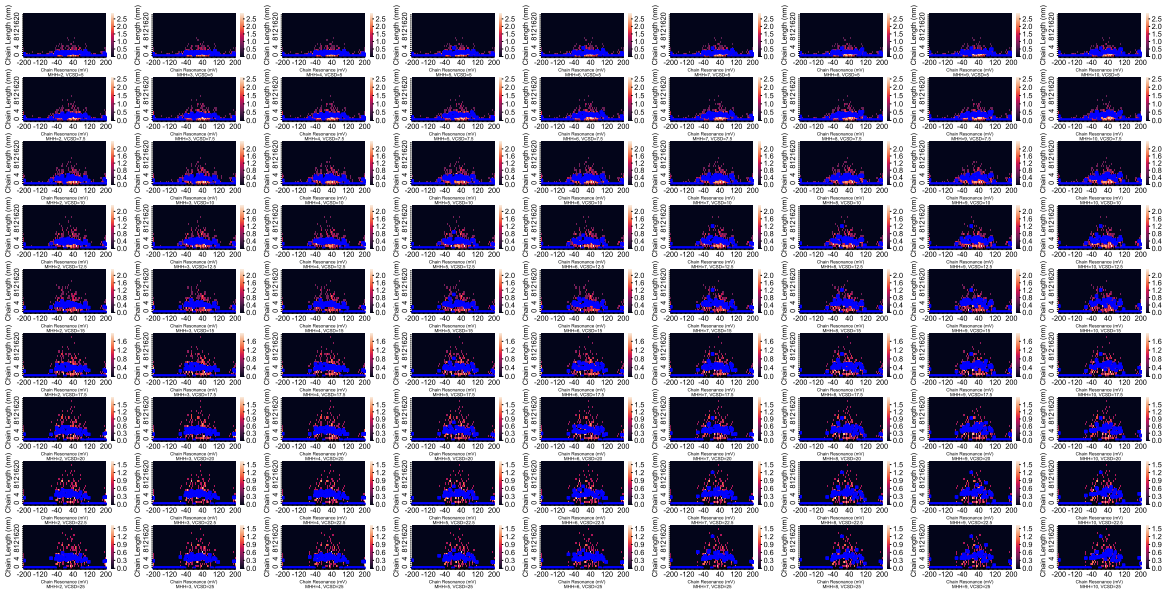

FIG. 5. Reproductions of Figure 4c using values of minimum histogram height (MHH) varying from 2 points (*left*) to 10 points (*right*) with vertical chain separation (VCS) varying from 5 pixels (*top*) to 25 pixels (*bottom*) in increments of 2.5 pixels. The main features of the graph, including a slight increase in the average length of chain at resonance energies closer to the Fermi energy, are preserved in all instances.